Engineering Similitude and Momentum Transfer Principles Applied to Shelterbelt Studies

N. P. Woodruff, D. W. Fryrear, and Leon Lyles
MEMBER ASAE ASSOC. MEMBER ASAE ASSOC. MEMBER ASAE

SHELTERBELTS, snow fences, strips of crops, and other bluff obstacles placed normal to the wind are widely used to protect crops and land from the ravages of wind. Investigations in the fields of meteorology, fluid mechanics, and aerodynamics have shown that a frictional drag is developed when a fluid (air or water) flows over a boundary surface. Placing a barrier in the path of the wind creates a new boundary surface of separation at an elevation approximately equal to the height of the barrier. This lessens the drag on the original surface and lowers the prevailing surface velocity. Considered from the standpoint of wind erosion control, benefits may accrue whenever the direct force of the wind on the soil is decreased.

The effectiveness of an obstacle in creating a new boundary and lowering the wind velocity depends on the object's shape, height, and porosity and upon the velocity of the wind. The problem of evaluating the individual effects of these variables is particularly amenable to solution by using wind tunnels, models, and similitude principles. Furthermore, since the problem is fundamentally one of fluid flow, the momentum and other fluid mechanics equations are applicable. Use of such techniques ignores silvicultural aspects of the shelterbelt problem but does provide controlled wind velocity, spacing, and porosity conditions.

This paper describes the use and applicability of engineering similitude principles for evaluating shelterbelt effectiveness. It also uses the momentum transfer relationships and the method of pitot-traverse measurements within the turbulent wake of a bluff obstacle, verified by actually measuring the drag of the model, to determine the drag and the drag coefficients for both model and prototype shelterbelts.

THEORETICAL CONSIDERATIONS

Similitude and Dimensional Analysis

Successful use of small-scale surface barrier models in a wind tunnel to predict the performance of a prototype barrier under natural conditions depends upon proper application of the theory of similitude. This theory as defined by Murphy (1)* deals with the proper design and construction, operation, and interpretation of test results of models and has been developed by dimensional analysis, an analytical tool attributed to Buckingham (2), from a consideration of the dimensions in which each of the pertinent quantities involved in a phenomenon is expressed. Dimensional analysis alone can only give qualitative relationships; however, if it is combined with experimental procedures, it will supply quantitative results and accurate prediction equations.

The first step in using models and the principles of similitude to predict prototype performance is to determine the pertinent variables. These variables are then grouped into a series of independent dimensionless pi (π) terms. The number of pi terms required to express a given phenomenon is determined from the Buckingham pi theorem which states that the number of dimensionless and independent quantities required to express the relationship among variables in any phenomenon is equal to the number of quantities involved minus the number of dimensions in which the quantities may be measured.

Pertinent variables involved in determining the velocities to the leeward of a prototype tree shelterbelt placed in the path of the wind are presented in Fig. 1. There are nine variables which may be expressed in three di-

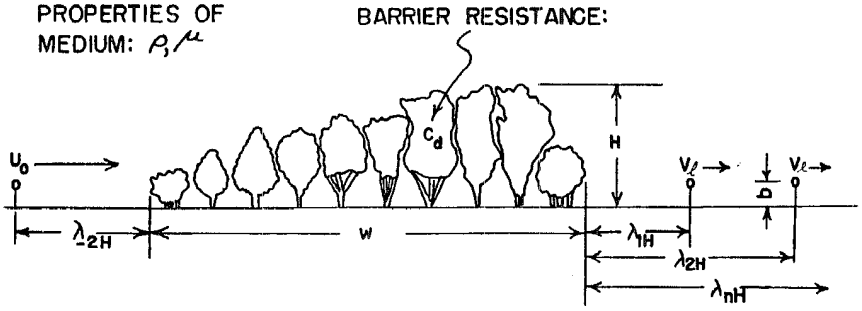

VARIABLES		DEFINITION	1/ DIMENSIONS
1.	V_ℓ	Leeward velocity	LT^{-1}
2.	H	Barrier height	L
3.	w	Barrier width	L
4.	b	Height of velocity measurement	L
5.	ρ	Air density	FT^2L^{-4}
6.	μ	Air viscosity	FTL^{-2}
7.	λ	Leeward distance	L
8.	C_d	Drag coefficient-barrier resistance	2/ (—)
9.	U_0	Upwind velocity	LT^{-1}

1/ L = length in feet
T = time in seconds
F = force in pounds

2/ (—) = dimensionless

FIG. 1 Pertinent variables describing wind flow over a tree shelterbelt.

Presented as Paper No. 61-702 at the Winter Meeting of the American Society of Agricultural Engineers at Chicago, Ill., December 1961, on a program arranged by the Soil and Water Division.
The authors—N. P. WOODRUFF, D. W. FRYREAR, and LEON LYLES—are agricultural engineers, Southern Plains Branch, Soil and Water Conservation Research Branch (ARS), USDA, Manhattan, Kans.
* Numbers in parentheses refer to the appended references.

This article is reprinted from the TRANSACTIONS of the ASAE (vol. 6, no. 1, pp. 41, 42, 43, 44, 45, 46 and 47, 1963), the Transactions of the American Society of Agricultural Engineers, Saint Joseph, Michigan

mensions: length, L; time, T, and force, F. According to the Buckingham pi theorem, six pi terms will be required and the equation

$$\pi_1 = f(\pi_2, \pi_3, \pi_4, \pi_5, \pi_6) \quad [1]$$

may be written.

The six pi terms describing this phenomenon may be written as follows:

$$\text{(a)}\ \pi_1 = \frac{V_l}{U_o} \qquad \text{(d)}\ \pi_4 = \frac{b}{H}$$

$$\text{(b)}\ \pi_2 = \frac{w}{H} \qquad \text{(e)}\ \pi_5 = C_d$$

$$\text{(c)}\ \pi_3 = \frac{\lambda}{H} \qquad \text{(f)}\ \pi_6 = \frac{\rho U_o H}{\mu}$$

Because equation [1] is entirely general, it would apply to any system which is a function of the same variables. Hence it would apply to a system involving models so that

$$\pi_{1m} = f(\pi_{2m}, \pi_{3m}, \pi_{4m}, \pi_{5m}, \pi_{6m}) \quad [2]$$

The model, to predict the prototype system, must be designed and operated so that

$$\pi_{2m} = \pi_2 \quad \pi_{4m} = \pi_4 \quad \pi_{6m} = \pi_6$$
$$\pi_{3m} = \pi_3 \quad \pi_{5m} = \pi_5$$

If all of these conditions are satisfied then the prediction equation is

$$\pi_1 = \pi_{1m} \quad [3]$$

In the problem at hand it follows that

$$\text{(a)}\ \frac{V_l}{U_o} = \frac{V_{lm}}{U_{om}} \qquad \text{(d)}\ \frac{b}{H} = \frac{b_m}{H_m}$$

$$\text{(b)}\ \frac{w}{H} = \frac{w_m}{H_m} \qquad \text{(e)}\ C_d = C_{dm}$$

$$\text{(c)}\ \frac{\lambda}{H} = \frac{\lambda_m}{H_m} \qquad \text{(f)}\ \frac{\rho U_o H}{\mu} = \frac{\rho_m U_{om} H_m}{\mu_m}$$

Equation (a) is the prediction equation. Equations (b) through (f) are the design and operating equations. The design conditions are indicative of the size of the model and prototype. The ratio of some pertinent length of the prototype to the corresponding length of the model is designated the length scale, n. Here the height of the barrier is used so that

$$H = n\, H_m \quad [4]$$

If equation [4] is solved for n and the relationship substituted into design equations (b), (c), and (d) then required lengths in the model are

$$\text{(b)}\ w_m = \frac{w}{n} \qquad \text{(c)}\ \lambda_m = \frac{\lambda}{n}$$

$$\text{(d)}\ b_m = \frac{b}{n}$$

A *true* model results if all design conditions are satisfied. If some cannot be satisfied, then it is necessary to use a distorted model. In the shelterbelt problem, since it is impossible to measure the porosity of a field shelterbelt, it is impossible to build a model that truly represents barrier resistance, C_d. It is therefore necessary to add a distortion factor β to equation (e) so

$$\text{(e)}\ C_{dm} = \beta C_d$$

Similarly it is often not possible to meet the operating conditions for a true model. Equation (f) is a good example. If it is assumed that air density and viscosity are equal for prototype and model, equation (f) reduces to

$$\text{(f)}\ U_{om} = n\, U_o$$

a result which is not desirable because if a scale factor of 50 is used, it means that the model must be tested under conditions of velocity equal to fifty times that of the prototype. However, equation (f) in its original form is the Reynolds number and fluid mechanics research (3) has shown that the effect of this number is constant above certain values. The model could therefore be operated at Reynolds numbers far below that indicated by equation (f) without affecting the prediction equation. However, to be sure that this is true for this particular problem, it was assumed that upwind velocity does have an effect, the model was tested at various wind speeds, and a distortion factor γ was added to equation (f) so that

$$\text{(f)}\ U_{om} = \gamma n\, U_o$$

Since any distortion in the pi terms violates the design and operating conditions, the prediction equation $\pi_1 = \pi_{1m}$ no longer is valid. It is therefore necessary to add a prediction factor δ so that $\pi_1 = \delta \pi_{1m}$, or in the problem at hand

$$\text{(a)}\ V_l = \frac{\delta V_{lm} U_o}{U_{om}}$$

Testing several models of varying porosity at different wind speeds will allow the relationship between distortion and prediction factors to be determined.

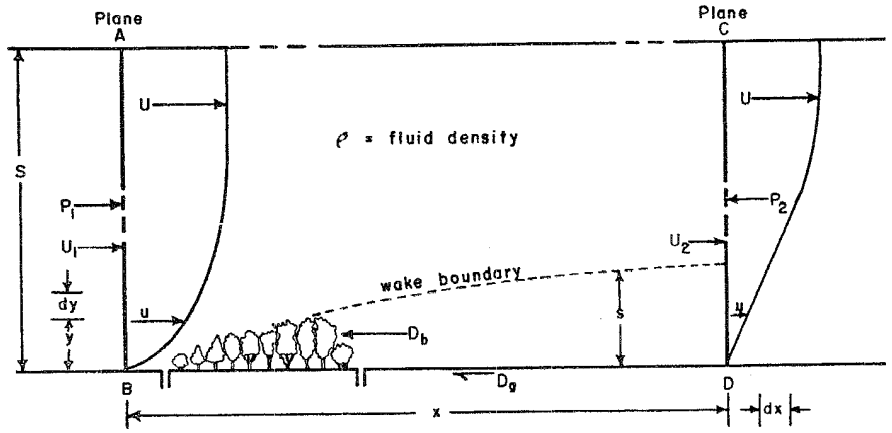

FIG. 2 Notation for development of momentum equation.

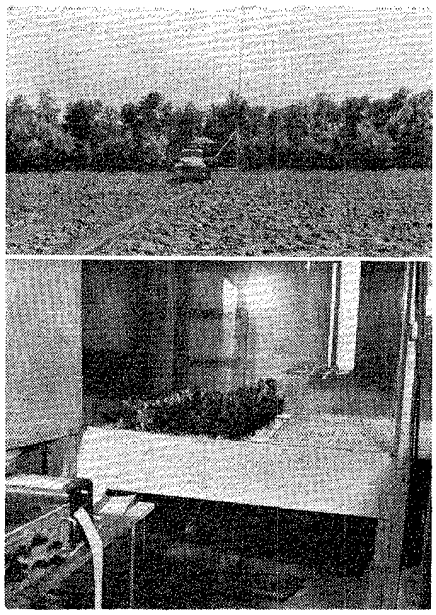

FIG. 3 Shelterbelts and equipment: (Top) Prototype and mobile tower with pitot tubes for measuring velocity profiles. (Bottom) A model in the tunnel with pitot tubes at the right and strain amplifying and recording equipment in the foreground.

Barrier Drag

Determining drag and the resistance coefficient of any type of barrier composed of growing plant material is a difficult problem. It is impossible to measure the porosity of either the prototype or model. It is therefore necessary to evaluate barrier resistance by resorting to techniques which measure the change in the air-flow patterns about the barriers.

Aerodynamicists have developed and used successfully, on both bluff and streamlined obstacles, techniques based on momentum transfer theories and velocity and pressure measurements within the turbulent wake to determine barrier drag or resistance to flow (4).

The situation where a shelterbelt is placed in a boundary layer in two-dimensional flow is shown diagrammatically in Fig. 2. Table 1 presents a definition and the dimension of each symbol used in developing the momentum

equation. In the usual considerations (5) of the momentum exchange between sections AB and CB, the momentum influx through the face AB is given by the integral

$$\rho\left[\int_o^S u^2\,dy\right]_{x=0}$$

through face CD by

$$\rho\left[\int_o^S u^2\,dy\right]_{x=x}$$

and through face AC by

$$U\rho\left\{\left[\int_o^S u\,dy\right]_{x=0} - \left[\int_o^S u\,dy\right]_{x=x}\right\}$$

According to momentum theory, the momentum influx plus the net force on the air within the boundaries equals the momentum efflux. A force accounting from Fig. 2 shows a net force

$$\int_o^S (P_1 - P_2)\,dy$$

due to pressure, a force D_g due to ground shear, and a force D_b due to barrier drag. Thus the basic momentum equation is

$$\rho\left[\int_o^S u^2 dy\right]_{x=0} + \int_o^S (P_1 - P_2)\,dy - D_b - D_g = \rho\left[\int_o^S u^2 dy\right]_{x=x} + U\rho\left\{\left[\int_o^S u\,dy\right]_{x=0} - \left[\int_o^S u\,dy\right]_{x=x}\right\} \quad \ldots\ldots\ldots\ldots [5]$$

An alternate form of this equation may also be written in a manner similar to that used by Betz (6) in aerodynamic research if sections AB and CD are considered to be parallel planes placed at right angles to the direction of motion, one in front and the other at some distance to the leeward of the barrier. Again considering a unit width in two-dimensional flow with negligible lift, u the velocity on the front and rear planes where $x = 0$ and $x = x$ is designated U_1 and U_2, respectively. If further the distance S is defined as the vertical distance to a point in the free airstream where $u = U = U_1 = U_2$, thus making the spillover or momentum efflux through the face AC equal to zero, the relation for drag from equation 5 is

$$D_b + D_g = \int_o^S (P_1 + \rho U_1^2)\,dy - \int_o^S (P_2 + \rho U_2^2)\,dy \quad \ldots\ldots\ldots\ldots [6]$$

These integrals may be restricted to a wake of depth, s, by utilizing the total head relationships

$$T_1 = P_1 + \tfrac{1}{2}\rho U_1^2$$
$$T_2 = P_2 + \tfrac{1}{2}\rho U_2^2$$

so that

$$D_b + D_g = \int_o^S (T_1 - T_2)\,dy + \tfrac{1}{2}\rho\int_o^s (U_1^2 - U_2^2)\,dy \quad \ldots\ldots\ldots\ldots [7]$$

Since the total head is constant along a streamline where viscosity and turbulence effects can be neglected, $(T_1 - T_2)$ is zero except in the wake and the first integral of equation [7] is confined to the wake. The second integral can be transformed by taking a hypothetical flow which is the same everywhere as the actual flow except in the wake. The total head in the wake is taken as T_1 and the pressure to be P_2, both the same as that in the undisturbed stream. This assumption implies the existence of a distribution of sources at the body and in the wake ahead of the rear measurement plane of total strength in terms of the mean rate of momentum transfer per unit width of flow, q, of

$$q = \int_o^s (U_2^* - U_2)\,dy \quad \ldots\ldots [8]$$

where U_2^* is assumed to be the X–component of velocity in the wake and is equal to

$$U_2^* = \sqrt{\frac{2\,(T_1 - P_2)}{\rho}}$$

use of the relationship expressed in equation [8] and the theory of streamline flow of an inviscid fluid permits writing equation [7] in the form

$$D_b + D_g = \int_o^s (T_1 - T_2)\,dy + \tfrac{1}{2}\rho\int_o^s (U_2^* - U_2)\,(U_2^* + U_2 - 2U)\,dy \quad [9]$$

where U is free stream velocity.

If the leeward plane is located some distance from the barrier, the second integral is negligibly small (7) and a very good approximation of drag can be determined from the expression

$$D_b + D_g = \int_o^s (T_1 - T_2)\,dy \quad [10]$$

From measurements of total head at each of the two planes at different values of y, pressures and velocities can be expressed as functions of y and the required integrations performed. Such computations will evaluate the total drag, $D_b + D_g$. The drag of the ground surface, D_g, in the zone from immediately leeward of the barrier to the leeward plane of measurement will in most cases be negligibly small in comparison to the drag of the barrier D_b; however, its approximate magnitude can be evaluated with additional pressure and velocity measurements made without the model in the tunnel or in the case of the prototype over terrain of similar roughness to that surrounding the shelterbelt.

The drag coefficient for a given barrier can be computed from the relationship

$$C_d = \frac{D_b}{\tfrac{1}{2}\rho\bar{u}^2 H} \quad \ldots\ldots\ldots [11]$$

Methods and Procedures

Experimental

The prototype used in this study was a ¼-mile-long, 10-row, 16-year-old field shelterbelt having an average effective height of 25 ft. The prototype leeward wind velocities used in the study were measured at several heights above ground and at several locations along a center line perpendicular to the belt length. Upwind velocities were measured at identical heights at a location free of the shelterbelt influence. Since a previous analysis of the data (8) had shown that the belt effectiveness varied with atmospheric stability conditions at time of measurement and could be classified under the following headings: (a) early forenoon and late afternoon (8:00 to 11:00 am and 3:30 to 6:30 pm, (b) midday (11:00 am to 3:30 pm, and (c) evening (9:30 to 11:30 pm), one representative set of data from each of the three classifications was selected from the fifteen complete and separate sets of data obtained during the months of July and August and used for making comparisons with the model. The shelterbelt and some of the velocity profiling equipment is shown in Fig. 3 (top). Detailed descriptions of experimental equipment and procedures may be found elsewhere (8).

A model of a 75-ft length of the cen-

TABLE 1. DEFINITION OF SYMBOLS FOR DEVELOPMENT OF MOMENTUM EQUATION

Symbols	Definition	Dimensions
ρ	Air density	$FT^2 L^{-4}$
u	Variable velocity	LT^{-1}
y	Vertical length	L
x	Horizontal length	L
U	Constant undisturbed velocity	LT^{-1}
S	Vertical distance to point in undisturbed airstream where $u = U$	L
P_1	Variable pressure on front plane	FL^{-2}
P_2	Variable pressure on leeward plane	FL^{-2}
D_b	Barrier drag per unit width of flow	FL^{-1}
D_g	Ground drag per unit width of flow	FL^{-1}
U_1*	Variable velocity on front plane	LT^{-1}
U_2*	Variable velocity on leeward plane	LT^{-1}
T_1	Total head on front plane $= P_1 + \frac{1}{2}\rho U_1^2$	FL^{-2}
T_2	Total head on leeward plane $= P_2 + \frac{1}{2}\rho U_2^2$	FL^{-2}
s	Depth of wake	L
q	Strength of source per unit width of flow	L^2T^{-1}
C_d	Drag coefficient — barrier resistance	(—)
$\bar{u}$	Mean upwind velocity in zone from ground	LT^{-1}
H	Barrier height	L

* Velocity designation for development of alternate or Betz (6) momentum equation.

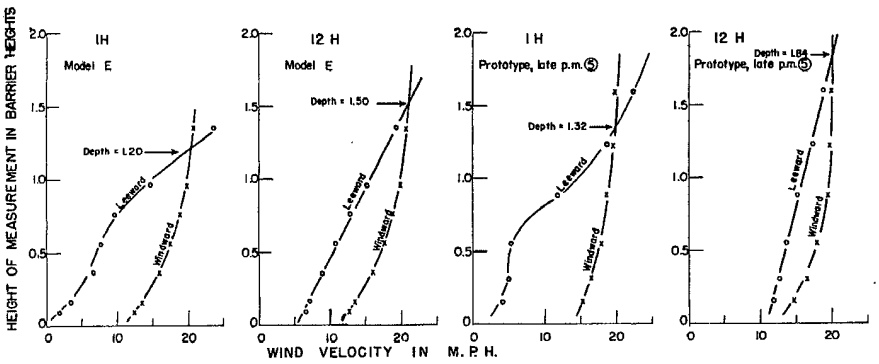

FIG. 4 Examples of windward and leeward wind profiles obtained for model E and prototype late afternoon (5). Point of intersection of leeward and windward profiles indicates approximate wake depths.

ter section of the prototype was constructed to a length scale of n equal 50. Combinations of green lichen glued to small spirea twigs were used for the tall Siberian elms. Smaller ash and coffee trees were duplicated from fern and wreath material commonly found in floral shops. Coniferous trees were constructed from balsa wood, green lichen, and florist wire using a spiral arrangement about the center trunk for the cedars and a "clothes tree" arrangement for the pine. A honeysuckle shrubbery row, dead but still standing, was duplicated using nylon brush bristles heated and bent to shape. The rows of trees were mounted on a lightweight styrofoam base. Three different porosity conditions were obtained and tested by thinning the original model.

The models were tested in a wind tunnel described previously (9). They were placed in the tunnel 40-ft downwind from the fan to provide sufficient length for boundary layer development. Wind-velocity profiles were measured with a staff of pitot tubes and an alcohol manometer. Measurements were made at identical locations to those

TABLE 2. MODEL DESIGNATIONS AND OPERATING CONDITIONS

Purpose of tests	Designation and relative porosity of models used*	Center of tunnel velocity, V_c	Mean velocity, $-2H$ upwind $\bar{u}$
Investigation of distorted upwind velocity, U_0	Model F (low)	6.2 mph	5.8 mph
	Model C (low)	12.5	11.3
	Model D (low)	20.1	17.6
	Model B (low)	29.9	26.1
Investigation of distorted barrier resistance coefficient, C_d	Model D (low)	20.1	17.6
	Model E (medium)	20.1	17.9
	Model A (high)	20.1	17.8

* Low = small openings, low wind penetrability. Medium = medium openings, medium wind penetrability. High = large openings, easily penetrated by wind.

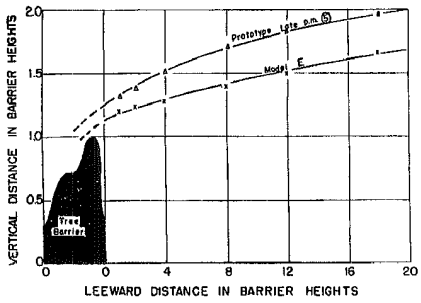

FIG. 5 Examples of wake depths as determined from the windward-leeward velocity profile intersection method. (Wake depths at the 12H location for other models and conditions of the prototype are given in Table 3).

of the prototype but scaled in accordance with the design equation.

Tests were run at four different wind speeds on models having a constant porosity to establish the relationship between the upwind distortion factor, γ, and the prediction factor, δ. Each model was considered in turn to be the prototype and equations (f) and (a) width U_0 and V_l measured at $0.16H$ above ground level were used to compute γ and δ. The relationship between porosity distortion, β, and the prediction factor, δ, was investigated by running a separate series of tests at constant upwind velocity on each of the three models having different porosities. Again each model was considered in turn to be the prototype and equations (e) and (a) were used to compute β and δ. Model designations, relative porosities, center of tunnel speeds, V_c, and mean upwind velocities, $\bar{u}$, at a location two times the height of the barrier ($2H$) windward are presented in Table 2.

Air temperatures were measured with copper-constantan thermocouples and an automatic potentiometer. Pres-

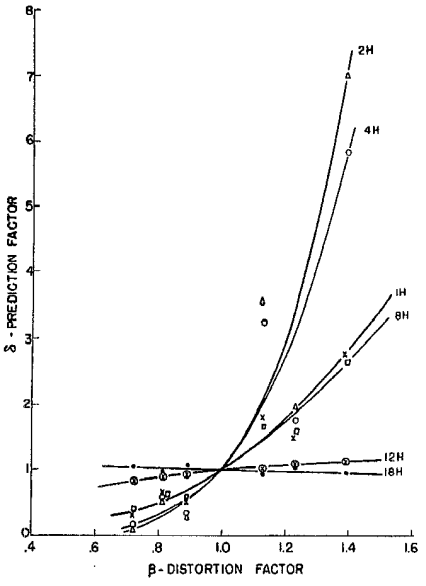

FIG. 6 Effect of distortion of barrier resistance on the prediction factor.

sure differentials were measured with piezometers and static tubes used with draft gages and manometers. Atmospheric pressure was measured with an aneroid barometer.

The actual drag of the model, used to verify computed drag, was measured by supporting the model on a vertical cantilever beam ¼ × ½-in. in cross section, which passed through the floor of the tunnel to a base resting on the floor of the laboratory. SR-4 strain gages were attached to the beam and the strain caused by the drag of the wind on the model was recorded with appropriate amplifying and recording instruments. These measurements were converted to force units from calibration curves established by applying known forces to the system. The model oriented in the tunnel, the pitot tubes, and the strain amplifier and recorder are shown in Fig. 3 (bottom).

Analytical

Velocity profile equations Relationships between height, y, and velocity, u, for use in equation [10] were determined graphically. The leeward data were plotted on several types of plotting paper to determine the general type of equation needed and the leeward location having the most easily described profile. Some examples of the type profile obtained are shown in Fig. 4. These plots show the difficulty in describing leeward profiles close to the barrier with a simple equation; however, at 12 H leeward the relationship is closely approximated within the limits measured by a linear equation, $y = mu - c$. A similar investigation of the −2 H upwind profile indicated that this profile was best described by an equation of the type $y = au^k$. The planes AB and CD of Fig. 2 were therefore taken at −2 H and 12 H and the momentum term of equation [10] was equal to

$$\left[\frac{\rho}{2}\frac{1}{a^{2/k}}\int_{z_o}^{s}\frac{2}{y^k}\,dy - \frac{1}{m^2}\int_{z_o}^{s} y^2 dy - \frac{2c}{m^2}\int_{z_o}^{s} y\,dy - \frac{c^2}{m^2}\int_{z_o}^{s} dy\right]$$

where the lower limit is taken at a negligibly small value slightly greater than zero (0.00095 ft, the value of roughness coefficient, z_o, for the gravel surface of the tunnel [12].

Pressure profile equations Plots of pressure differential, $P_1 - P_2 = \Delta P$ versus height, indicated that ΔP increased with height in the layer from the surface up to approximately 0.5 H; then a reversal occurred as the free airstream above the barrier was approached. The lower portion of this curve could be approximated by an equation of the form $y = d\,\Delta P^q$. The difference in pressure in the upper zone was found to contribute an insignificant amount to the pressure term involved in equation [10] and was therefore ignored. The pressure term in equation [10] was then computed from the integral

$$\frac{1}{d}1/q\int_{z_o}^{s} y^{1/q}\,dy$$

Wake depths Because the instruments used in this study were not sensitive enough to determine the wake boundary accurately, the approximate boundary was taken at the height of intersection of the upwind and downwind profile (Fig. 4). Examples of the wake boundaries as determined for one of the models and one condition of the prototype are shown in Fig. 5. The average depth of wake at the 12 H leeward location was 1.5 H for the models and 1.8 H for the prototype.

Determination of mean $\bar{u}$ Mean $\bar{u}$ for use in the drag coefficient equation was determined by integrating the equation of the upwind velocity profile to the limits of wake depth at 12 H leeward according to the mean value of a function formula [11]

$$\Phi\overline{X} = \int_{z_o}^{s}\frac{\Phi X\,dy}{s - z_o}$$

Determination of predicted V_l Equations (e) and (f) were used to compute β and γ between field prototype and the models. n was equal to 50 and the computed rather than the measured value of C_d was used. The prediction factor δ was computed from the appropriate relationship for each leeward location. (See Table 3 and equation [12]. Predicted V_l was computed from equation (a).

Results

Distortion (Prediction Factor Relationships)

Figs. 6 and 7 show the prediction factor, δ, to be a function of both γ and β. The relationship was established by multiple-curvilinear regression procedures. The general form of the equation was

$$\log \delta = a + b \log \gamma + e \log \beta \quad [12]$$

Values of a, b, and e for the various leeward locations are presented in Table 3.

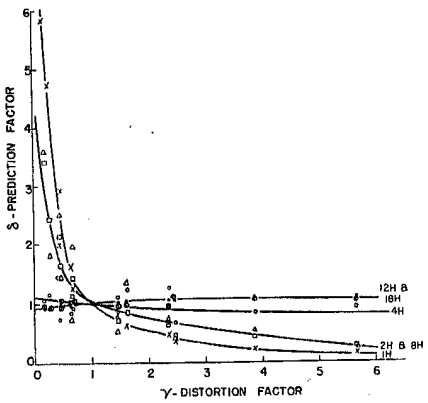

FIG. 7 Effect of distortion of upwind velocity on the prediction factor.

Barrier Drag

The computed and measured drag and drag coefficients for the models and the computed values for measurements during three different times of the day for the prototype are given in Table 4.

Measured and computed barrier drag agree fairly well. Except for model A, all the computed drag coefficients are larger than measured. Largest and smallest difference noted between computed and measured drag coefficients occurred for model C and model E, respectively.

The average computed resistance coefficient for the prototype was 0.56. The average for the first model constructed, here designated as models B, C, D, F, was 0.76. However, model A, the most porous model, with a computed resistance coefficient of 0.55 was close to a true model insofar as resistance was concerned.

The close agreement among the three prototype coefficients, each computed from a separate set of measurements, provides some evidence that they are reasonable for the particular prototype.

Predicted and Measured Leeward Velocity Comparisons

A graphical comparison of predicted and measured velocity ratios at 0.16 H above ground level is shown in Fig. 8. Predicted values were computed for only four of the six models tested and compared with the three sets of prototype measurements.

Predicted and measured leeward velocities generally agree. Predicted values are lower than measured with the exception of locations near the belt during the evening. The prototype measurements made in the late afternoon and evening period are in closer agree-

TABLE 3. CURVILINEAR REGRESSION CONSTANTS a, b, AND e FOR EXPRESSING δ AS A FUNCTION OF β AND γ

Values of constants	Leeward location					
	1 H	2 H	4 H	8 H	12 H	18 H
a	1.0000	1.0000	1.0000	1.0000	1.0000	1.0000
b	−0.0360	−0.0044	−0.0091	−0.0039	+0.0060	+0.0020
e	+2.97	+5.55	+5.39	+2.70	+0.41	−0.15

ment with predicted values than are the measurements made during the midday period.

There is no definite evidence that one model or one operating condition was better than another. However, model A with a resistance coefficient close to that of the prototype and model B, a less porous model tested at a wind speed much higher than the prototype, seem to predict measured leeward velocities more closely than do other models.

Discussion

Following is a discussion of some of the results and techniques used in this study.

Mathematical interpretation of the velocity profiles is one of the first problems encountered. Here a log-log or power relationship was used to describe the upwind profile. This type of equation is often used; however, many profiles obtained under different conditions of atmospheric stability or surface roughness can be better described with the exponential or semilog relationship. Choice of a relationship must therefore be determined on an individual case basis. The linear relationship used for the 12 H leeward profile is simple and seems adequate; however, it must be remembered that the velocity at some point very near the ground must be zero, so the linear relationship must be confined within definite limits above the surface.

In this study the leeward profile was taken at the 12 H location principally because this profile was easy to describe mathematically. Theoretically, however, the momentum equation should apply between any two planes. To check this, the drag of model E was computed with data from profiles at 8 H and 18 H. The resulting drag coefficients were 0.652 and 0.595, respectively. The measured value was 0.655; thus the theory does apply so long as fairly accurate profile equations can be determined.

Accurate determinations of wake depth are vitally important in using the theories presented in this study. Measurement is extremely difficult in the case of the prototype. The upwind and leeward profile intersection point method used here appears to be fairly reliable. Depths determined were in good agreement with previous results (10) and with those reported by other investigators (4). They also generally agree with the smoke photograph of the wake of a bluff vertical plate shown in Fig. 9. This photograph was made for another study and is rather poor but does show that wake boundary for a bluff object in a turbulent boundary layer increases in depth for some distance to the leeward of the object.

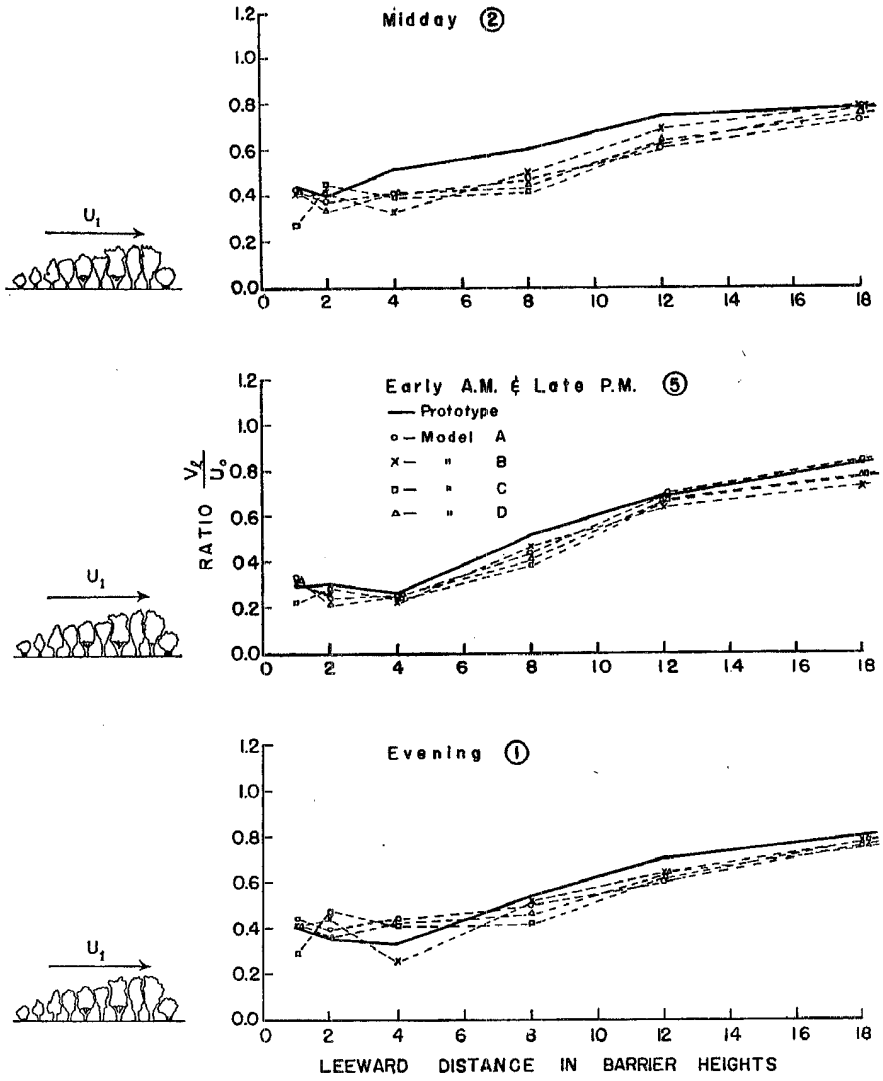

FIG. 8 A comparison of predicted and measured leeward velocity ratios at 0.16H above ground level. Prototype measurements were made during different atmospheric stability conditions commonly occurring as the day progresses.

Table 4 does not include values of D_g for the prototype. Preliminary calculations indicated this force to be insignificant in relation to the large value of prototype barrier drag. Likewise, pressure forces were not evaluated for the field condition. While both of the forces were significant in relation to the small barrier drag in the tunnel where flow was confined, they were not significant in the open field condition.

In computing the prediction factor between models and field prototype, it was necessary to extrapolate equation [12] considerably beyond the limits of the data used in its derivation. This was caused by the very small values of γ obtained from equation (f) with the use of a scale factor of 50. This extrapolation seems justified in view of results of previous research (10, 3) which show the ratio V_l/U_o to be

TABLE 4. MEASURED AND COMPUTED DRAG (D_b) AND DRAG COEFFICIENT (C_d) FOR MODEL AND PROTOTYPE

Barrier	Wake depth, s	Computed			Measured	Mean upwind	C_d		Ratio = C_d computed / C_d measured
		$D_b + D_g$	D_g	D_b	D_b	$\bar{u}$	Computed	Measured	
	ft	lb/ft	lb/ft	lb/ft	lb/ft	ft/sec			
Model A	0.69	0.2193	0.0051	0.2142	0.2260	26.2	0.549	0.579	0.95
B	0.76	0.5722	0.0120	0.5602	0.4910	38.3	0.704	0.617	1.14
C	0.77	0.1202	0.0017	0.1185	0.0800	16.6	0.774	0.523	1.48
D	0.77	0.2847	0.0051	0.2796	0.2640	25.8	0.762	0.719	1.06
E	0.75	0.2593	0.0051	0.2542	0.2483	26.3	0.672	0.655	1.02
F	0.78	0.0323	0.0004	0.0319	0.0249	8.5	0.788	0.617	1.26
Prototype Midday two	46.00	2.33	....	2.33	....	16.2	0.548	....	....
Evening	42.50	8.74	....	8.74	....	24.1	0.542	....	....
Early a.m. & late p.m. five	46.00	12.51	....	12.51	....	27.5	0.596	....	....

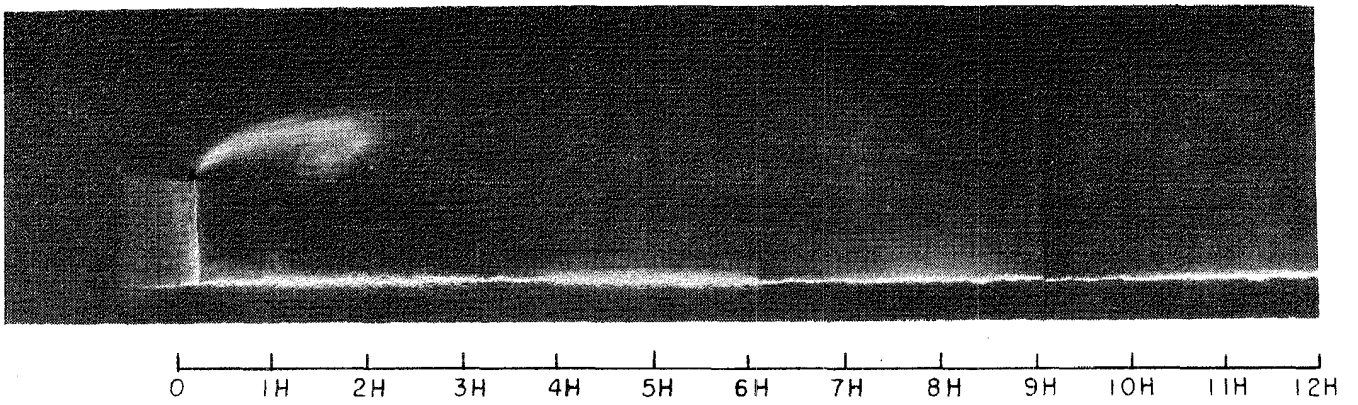

FIG. 9 Chemical smoke patterns to the leeward of a thin bluff vertical plate.

nearly independent of upwind velocity and the drag coefficient of a barrier to be independent of the Reynolds number of flow. These previous research results seem to be further verified here by the very small value of the coefficient for γ, the distortion factor for the upwind.

The applicability and reliability of the wake measurement-momentum transfer method for computing barrier drag is supported by the general agreement between measured and computed drag. It is further justified in the succeeding step where prototype leeward velocities are predicted. Here large errors in evaluating drag coefficients would have led to much larger differences between measured and predicted values than were obtained.

The larger differences between measured and predicted leeward velocity ratios shown in Fig. 8 for the midday period are probably due to differences in stability conditions between the tunnel and the atmosphere. The early forenoon and late afternoon and the evening periods were characterized by relatively stable, less turbulent winds more nearly comparable to the tunnel. Midday winds were turbulent and gusty. It is probable, therefore, that a distortion of turbulence exists between tunnel and atmosphere. Another Pi term including the turbulence variables and another distortion factor probably would improve the predicted-measured relationship for the midday period.

Conclusions

This study makes contributions in two areas pertaining to shelterbelt research and to field evaluation of shelterbelts. First, it demonstrates that data obtained from models in a wind tunnel interpreted in accordance with accepted engineering similitude principles can be used to evaluate field shelterbelt effectiveness satisfactorily. Second, it provides a method whereby the drag and the resistance coefficients for field shelterbelts can be determined from vertical velocity profile measurements made at two locations, one windward and one leeward of the shelterbelt. Both of these contributions should be useful in reducing the amount of work necessary in future evaluations of the effectiveness of existing tree shelterbelts in the Great Plains.

References

1 Murphy, Glenn. Similitude in engineering. The Ronald Press Co., N.Y., 302 p., 1950.

2 Buckingham, E. Model experiments and forms of empirical equations. Trans. Amer. Soc. Mech. Engrs. 37:263-296, 1915.

3 Rouse, H. Fluid mechanics for hydraulic engineers. McGraw-Hill Book Co., New York, 1938.

4 Goldstein, S. Modern developments in fluid dynamics. Oxford Press, Oxford, England, vol. I & II, pp. 256-265, 561-600, 1950.

5 Binder, R. C. Advanced fluid mechanics. Prentice-Hall, Inc., Englewood Cliffs, N.J., vol. II, pp. 62-86, 1958.

6 Betz, A. Zeitschr. f. Flugtechn. u. motorluftschiffahrt, 16, pp. 42-44, 1925. See also Goldstein, S. Modern developments of fluid dynamics, Oxford Press, Oxford, England, vol. I, pp. 258-59, 1950.

7 Fage, A. and Jones, L. J. On the drag of an aerofoil for two dimensional flow. Proc. Roy. Soc. Series A, vol. III, pp. 592-603, 1926.

8 Woodruff, N. P., Read, R. A., and Chepil, W. S. Influence of a field windbreak on summer wind movement and air temperature. Kans. Ag. Exp. Sta. Tech. Bul. 100, pp. 4-6, June 1959.

9 Zingg, A. W. and Chepil, W. S. Aerodynamics of wind erosion. **Agricultural Engineering** 31:279-282-284, 1950.

10 Woodruff, N. P. and Zingg, A. W. Wind tunnel studies of fundamental problems related to windbreaks. USDA, SCS-TP 112, p. 14, 1952.

11 Granville, W. A., Smith, P. F., and Langley, W. R. Elements of calculus. Ginn & Co., New York, 1941.

12 Zingg, A. W. Wind tunnel studies of the movement of sedimentary materials. Proceedings of the Fifth Hydraulics Conference. Bul. 34, State Univ. of Iowa, Studies in Engineering, pp. 111-135, 1953.